buildings

MDPI

Article

Deformation and Strength Characteristics of Marine Soft Soil Treated by Prefabricated Vertical Drain-Assisted Staged Riprap under Seawall Construction

Xue-Ting Wu [1,*], Jun-Ning Liu [1] and Zhi-Min Xie [2]

[1] Faculty of Engineering, China University of Geosciences, Wuhan 430074, China
[2] China Railway Eryuan Engineering Group Company Limited, Chengdu 610031, China
* Correspondence: wuxueting@cug.edu.cn

Abstract: Prefabricated vertical drains (PVDs) with staged riprap preloading have been widely used in soft soil ground improvement and embankment construction. However, ground treatment effectiveness evaluation is still a difficult problem due to multiple factors. Considering this, in situ monitoring and numerical simulation were conducted to study the deformation and strength characteristics of marine soft soil ground treated by PVD-assisted staged riprap under the Lingni Seawall construction in China. Monitoring and analysis of results showed that use of PVD-assisted staged riprap resulted in a good improvement effect. In particular, in the PVD-treated zone within 10 m in depth, corresponding to a half-length of the PVD, the average radial degree of consolidation reached up to 75–100%, and the soil strength increased significantly by 200–700%. Moreover, numerical simulation showed that the linear 1-dimensional drain element of PVD closely met the engineering accuracy requirements with good consistency with the monitoring data. Compared with a totally solid element model, the numbers of elements and nodes were reduced and the calculating efficiency and model accuracy were increased by using a PVD linear element, which provides a basis for building large complex finite element models.

Keywords: deformation; strength; marine soft soil; prefabricated vertical drain (PVD); staged riprap

check for updates

Citation: Wu, X.-T.; Liu, J.-N.; Xie, Z.-M. Deformation and Strength Characteristics of Marine Soft Soil Treated by Prefabricated Vertical Drain-Assisted Staged Riprap under Seawall Construction. *Buildings* **2023**, *13*, 2322. https://doi.org/10.3390/buildings13092322

Academic Editors: Chao He and Erwin Oh

Received: 6 August 2023
Revised: 2 September 2023
Accepted: 9 September 2023
Published: 13 September 2023

Copyright: © 2023 by the authors. Licensee MDPI, Basel, Switzerland. This article is an open access article distributed under the terms and conditions of the Creative Commons Attribution (CC BY) license (https://creativecommons.org/licenses/by/4.0/).

1. Introduction

With the development of the economy, many coastal cities need to carry out land reclamation [1]. Constructions on deep soft soils will result in significant post-construction settlement. Generally, the time allocated for treating the soft ground constitutes 30% to 40% of the overall process [2,3]. According to Terzaghi's consolidation theory (1923) [4], the consolidation time is proportional to the square of the drainage distance. Therefore, setting vertical drainage wells in natural soil layers is a commonly used method to increase the number of drainage channels and to shorten drainage distances [5]. Prefabricated vertical drains (PVDs) have the advantages of being low carbon and of saving energy in the production process at a lower cost. Therefore, PVD-assisted preloading has been recognized as an efficient and economical soft ground improvement technique [6].

However, there is some confusion and uncertainty about PVD performance as well as appropriate project design and construction procedure due to various factors, including: (i) the smear zone [7]; (ii) bulking and clogging of the PVD [8]; (iii) soil inhomogeneity; and (iv) limitations of calculation theory. These factors have been identified in field operations and laboratory tests [9,10], and can lead to the relatively low reliability of project design [11].

In terms of facilitating PVD-assisted ground treatment, model testing, in situ monitoring, and numerical simulation are frequently used in evaluation by research and industrial communities [12,13]. Bo (2016) [10] demonstrated that current model-testing techniques for evaluating the optimal performance of PVD were limited. In situ monitoring, which involves confirming whether the required ground conditions have been achieved, can represent the actual situation considering the soil profile's heterogeneity, the preloading, and the PVD used [14]. Consequently, it is considered a reliable method for accurately evaluating PVD performance [15].

Furthermore, numerical simulation has been widely employed to address the limitations of analytical approaches [16,17] in complex PVD-assisted preloading projects [18,19]. However, determination of the properties of the smear zone is a challenging task because of many uncertainties [20]. PVDs have usually been modeled as solid elements [21,22] in a plane-strain state [23], resulting in a large amount of calculation and a non-correspondence at the ground geometric position to the prototype model. Kan (2021) proposed a linear drain element for a PVD, representing it as a stagnant plane-strain unit cell [24]. Therefore, appropriate modeling of PVDs is very important in the numerical simulation of PVD-assisted drainage consolidation foundation treatment. It is a challenge to find a PVD model that includes consideration of the drainage consolidation effect, and, at the same time, avoids increasing the finite element nodes and the plane-strain equivalent transformation.

In this study, staged riprap loading combined with use of a PVD in the Lingni Seawall project was considered. The survey and monitoring data were extracted and used to develop a numerical model, aiming at minimizing the number of elements and nodes and increasing the computational efficiency and model accuracy without using the plane-strain equivalent transformation. The model used included a self-defined linear 1-dimensional PVD drain element by secondary development based on the UEL subroutine using the commercially available ABAQUS finite element software. The reliability of this simulation model was verified by comparing the outcomes with data obtained from the field. The consolidation, settlement, deformation, and strength characteristics of the PVD-treated soft ground were identified.

2. Project Description and Geological Characterization

2.1. Project Description

The Lingni Seawall project is located in Wenzhou, Zhejiang Province, China, as shown in Figure 1. The Lingni Seawall is a stone embankment connecting Lingkun Island and Niyu Island, with a total length of about 14.5 km (extending from N0 + 000 to N14 + 509). The embankment crest width is 10.5 m, with a crest elevation of 5.63 m according to the National Height Datum 1985 of China. The site is located in the Wenzhou Shoal of Wenzhou Bay, where the soil is often saturated. A combined PVD using a staged riprap preloading technique was adopted to reinforce the soft ground comprising the seawall foundation. The foundation treatment cross-section of the Lingni Seawall and the quincunx equilateral triangle pattern of the PVD are shown in Figure 2. The cross-section of the PVD used in this project was a rectangle of 100 mm width and 5 mm thickness.

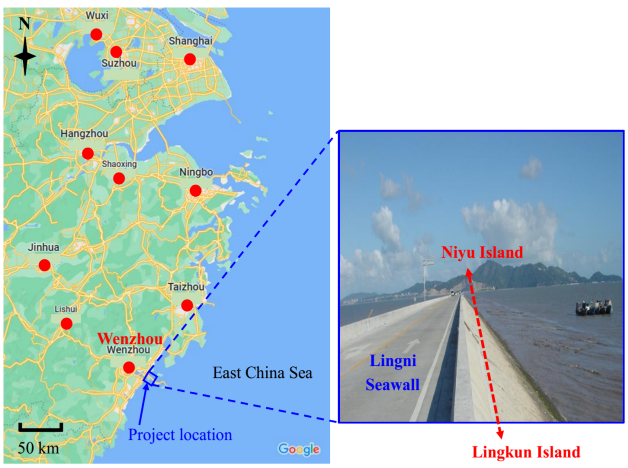

Figure 1. Location of the Lingni Seawall (Google Maps).

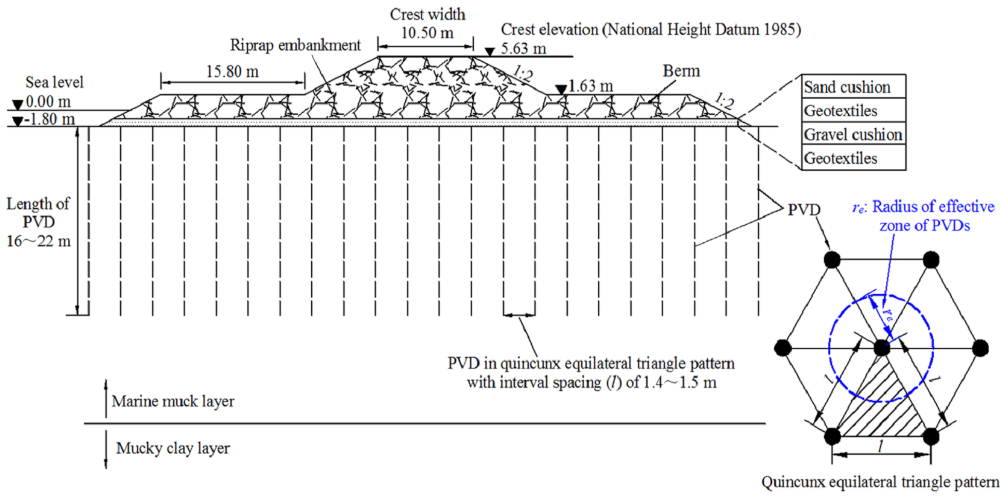

Figure 2. Foundation treatment cross-section of the Lingni Seawall.

2.2. Site Geological Characterization

The underlying ground exploration and boring data revealed that the profile was mainly comprised of soft marine soil [25,26] (Figure 3). Generally, the profile can be divided into four layers; the soil parameters corresponding to each layer are detailed in Table 1. It must be noted that, along the seawall, remarkable variations in the thicknesses and heterogeneity of the soil profile were observed. Therefore, the characteristics of each cross-section were extracted from the corresponding exploration data and used in this study. In total, 60 sections equipped with ground settlement observation out of 63 monitoring sections were selected. Furthermore, there were three in situ observation sections [27], namely, section N3 + 850, section N5 + 850, and section N11 + 050. The N5 + 850 cross-section is presented here, while sections N3 + 850 and N11 + 050 were analyzed and are discussed in the results. The soil parameters of section N5 + 850 are listed in Table 2.

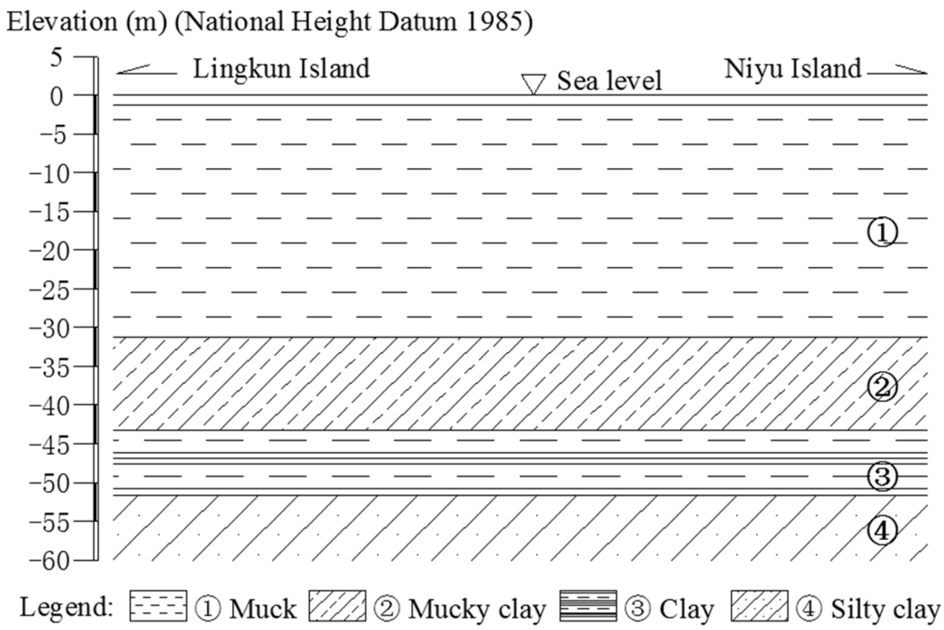

Figure 3. Typical stratum profile of marine soft soils at project site.

Table 1. Soil parameters of each layer at project site.

Soil Layer	Thickness, h (m)	Allowable Bearing Capacity, F (kPa)	Ultimate Friction Resistance, τ (kPa)
Muck	3.8–33.5	45–60	10–12
Mucky clay	1.0–21.7	60–70	15–18
Clay	1.8–22.0	80–100	20–25
Silty clay	1.5–30.3	140–180	33–45

Table 2. Soil parameters of section N5 + 850 of Lingni Seawall.

Soil Layer	Thickness, h (m)	Unit Weight, γ (kN/m^3)	Natural Water Content, ω (%)	Modulus of Compression, Es^* (MPa)	Compression Index, Cc^*
Muck	30.0	16.17	65.6	1.88	0.556
Mucky clay	12.0	17.15	48.7	2.48	0.391
Clay	8.5	17.64	37.2	2.92	0.228
Silty clay	>10.0	18.33	30.9	3.70	0.121

* This value corresponds to the compressive stress between 100 kPa and 200 kPa.

3. Methods

Field monitoring and measurements were used to investigate the variations and regularity in the deformation and strength of the soft soil ground after applying the ground improvement. Moreover, numerical simulation was carried out based on the monitoring data, which can provide a reliable reference to guide similar projects during the design and construction stages [28].

3.1. In Situ Monitoring and Measurement

For controlling the riprap rate and monitoring the consolidation effectiveness of the Lingni Seawall, in situ monitoring and measurements of the ground surface settlement, the layered settlement, the horizontal displacement, the hydrostatic water level and the pore water pressure, and a field vane shear test, were performed. The layout and symbols of the monitoring sensors and measurement apparatus deployed in section N5 + 850 are shown in Figure 4. All the monitoring holes and sensors were embedded in the center of the area surrounded by the PVDs. The depth of the monitoring hole was about 30 m, equal to the thickness of the marine muck layer, which was considered the main deformation stratum. Settlement meters were set at 2 m intervals in the layered settlement monitoring hole. At the pore water pressure monitoring hole, pore water pressure piezometers were set every 3 m in the PVD-treated zone and every 5 m in the zone without PVD (the zone below the PVD-treated zone, namely, the non-PVD zone in this study).

Monitoring was performed for more than two years (about 750 days). Observations were carried out daily during the staged riprap loading until the settlement value was less than 2 mm/d. After that, monitoring was carried out once every 3 to 14 days depending on the observation results. Based on the monitoring data of the Lingni Seawall, the consolidation deformation characteristics, the dissipation regulation of the pore water pressures, and the strength improvement were analyzed both for the PVD-treated zone and for the non-PVD zone. The degree of consolidation and the consolidation coefficient of the soft marine soil were calculated and inversely evaluated using the monitoring data.

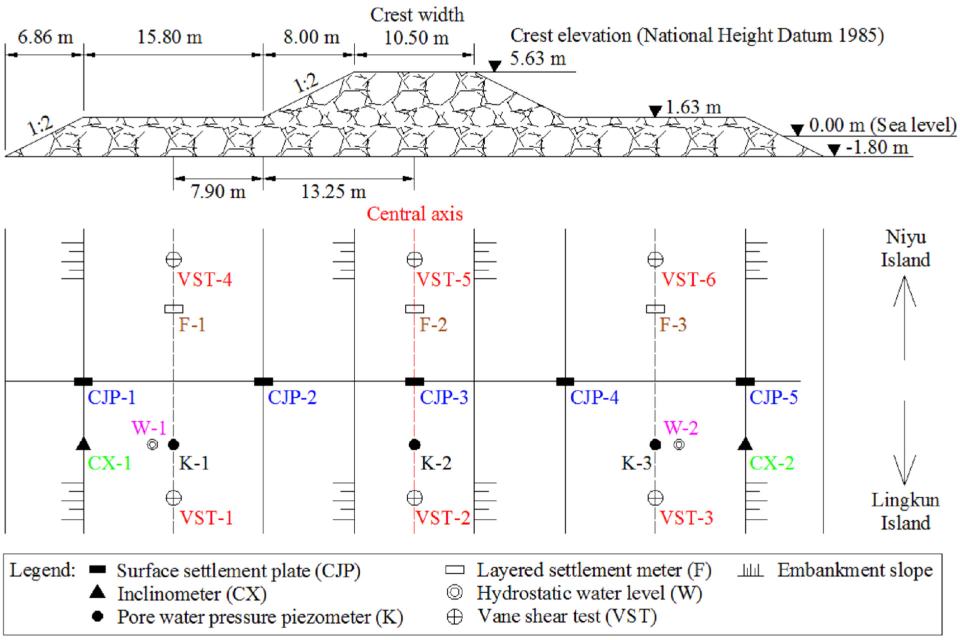

Figure 4. Layout of monitoring sensors and measurement apparatus in section N5 + 850.

3.2. Numerical Simulation

3.2.1. Fundamental Assumptions

In this numerical simulation model, factors such as the seismic load, the traffic load, and the soil temperature sensitivity were ignored. In order to make the model calculation and analysis more straightforward, the following assumptions were made in this study: (i) the surface distribution of the riprap filling was uniform, ignoring the influence of temperature; (ii) the surface of each soil layer in the modeling section was relatively horizontal, and the soil material was isotropic; (iii) the stability of the simulated project was determined by the convergence of the model calculation results.

3.2.2. Model Scale and Boundary Conditions

A finite element model was established using ABAQUS software (Ver. 6.14, SIMULIA, Dassault, France). Considering the symmetry of the numerical model [22], only half of the Lingni Seawall was modeled. The deformation of the marine soft soil ground mainly occurred in the range of the soft soil layers under the Lingni Seawall, including the muck layer with a thickness of 30 m and the mucky clay layer with a thickness of 12 m. Furthermore, previous studies [29,30] have indicated that the horizontal width of the simulation model can be set at about two times the half-width of the embankment. Therefore, the model boundaries were set at 72 m from the embankment center in the horizontal direction and 42 m below the ground surface in the vertical direction to avoid boundary effects.

The left boundary of the model was the center line of the embankment. The left and right boundaries were undrained and fixed in the horizontal direction, while the bottom boundary was fixed in both the vertical and horizontal directions, and the upper boundary was a free surface. In the process of numerical simulation, the 3-dimensional problem was transformed into a 2-dimension plane strain problem. The mesh refinement was divided into elements by the plane strain pore pressure element type (CPE8RP), which meant that the 8-node quadrilateral element mesh was obtained by secondary reduced integration through structured mesh division. Furthermore, the meshes were more dense throughout the entire soil layers inside the range of the embankment than in the other areas. The riprap loading was applied step-by-step in the simulation process. The numerical model, assigned finite element mesh, and the boundary conditions of the embankment are illustrated in Figure 5.

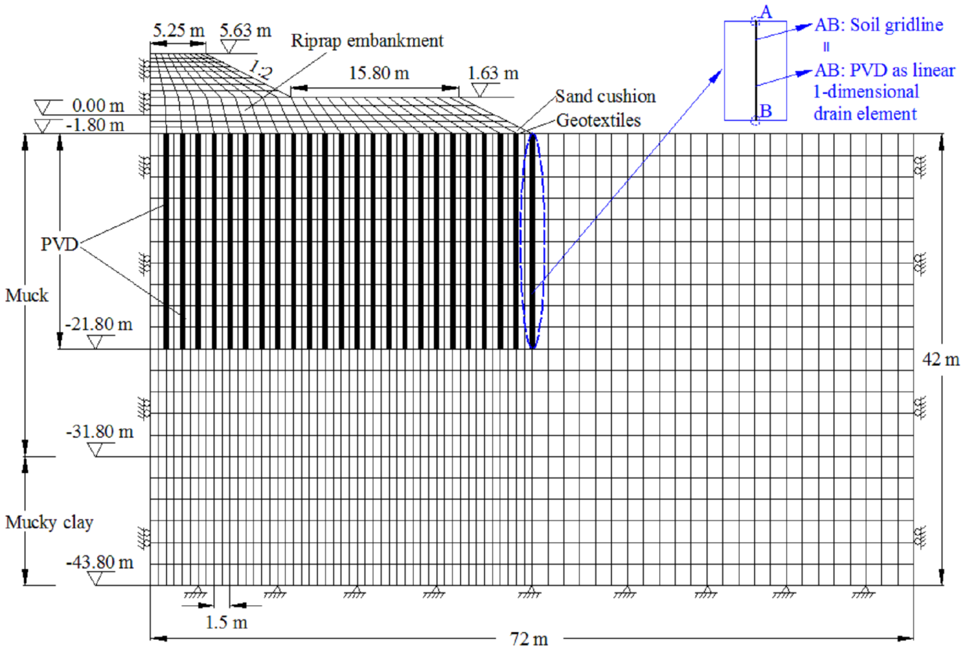

Figure 5. Finite element model with boundary conditions and mesh technology of the Lingni Seawall.

Furthermore, the PVD model was constructed using a secondary development process with a self-defined drainage plate element based on the UEL subroutine provided by ABAQUS [31]. Unlike in other studies, the PVD was defined as a line element rather than a solid element [23], considering that the PVD cross-section was relatively small compared to its length and spacing. Therefore, by minimizing the number of elements and nodes, the PVD was modeled as a 1-dimensional drain element (AB) (Figure 5).

3.2.3. Constitutive Model

The materials involved in the Lingni Seawall numerical simulation included the PVD, geotextile, sand cushion, riprap, muck, and mucky clay. The PVD was modeled as a 1-dimensional linear elastic model. The geotextile was also set as an elastic material model and embedded in soils by beam element. The sand cushion and the riprap were represented by a Mohr–Coulomb elastic–plastic model. A modified Cam-Clay model was used for the muck and mucky clay.

3.2.4. Model Parameters

The elastic model parameters of the PVD were as follows: (i) the cross-sectional area of the PVD was 500 mm^2; (ii) the length of the PVD was 20 m; (iii) the modulus of elasticity of the PVD was 10 MPa; and (iv) the coefficient of permeability of the PVD was 0.001 cm/s.

Furthermore, as an elastic material, the geotextile was modeled using a beam element with a modulus of elasticity of 30 MPa.

The Mohr–Coulomb criterion was used to describe the sand cushion and the riprap with the parameters summarized in Table 3.

Table 3. Mohr–Coulomb model parameters for the sand cushion and riprap.

Mohr–Coulomb Model Parameters	Sand Cushion	Riprap
Unit weight, γ (kN/m^3)	18.3	21.0
Cohesion, c (kPa)	1.0	29.3
Internal friction angle, ϕ (°)	40.0	36.4
Modulus of elasticity, E (MPa)	20	50

A modified Cam-Clay model was used for the muck and mucky clay [32]. The modified Cam-Clay model included the following parameters: unit weight (γ), coefficient of permeability (k_h), cohesion (c), internal friction angle (ϕ), compression index (Cc), Poisson's ratio (ν), void ratio ($e1$), critical stress ratio (M), slope λ (compression indicator), slope κ (swelling indicator). M, λ and κ can be calculated using Equations (1) to (3), respectively. The modified Cam-Clay model parameters for all the soil layers in this numerical code are summarized in Table 4.

$$M = 6\sin\phi/(3 - \sin\phi) \tag{1}$$

$$\lambda = Cc/ln10 \tag{2}$$

$$\kappa = 0.2\lambda \tag{3}$$

Table 4. Modified Cam-Clay model parameters for soil layers in numerical code.

Modified Cam-Clay Model Parameters	Muck	Mucky Clay
Unit weight, γ (kN/m^3)	16.17	17.15
Coefficient of permeability, k_h (10^{-4} m/d)	8.64	4.23
Cohesion, c (kPa)	4.0	8.1
Internal friction angle, ϕ (°)	15	25
Compression index, Cc	0.556	0.391
Poisson's ratio, ν	0.35	0.33
Void ratio, $e1$ (when p = 1 kPa)	1.60	0.78
Critical stress ratio, M	0.566	0.983
Slope λ (compression indicator)	0.24	0.17
Slope κ (swelling indicator)	0.048	0.034

3.2.5. PVD Modeling

A plane strain unit cell using a linear drain element of PVD was introduced by Kan (2021) [24], where the effect of drain size was converted to an equivalent reduction in the size of the smear zone surrounding the drain. In contrast, the adopted method did not assume a plane strain equivalent transformation but considered the drainage consolidation effect of the PVD, which avoided the need to increase the nodes. Only the axial force and the permeability of the PVD were included in the model, while the weight, shear, and torsion properties were not considered.

For the PVD element, the axial force and the water flow velocity along the rod length will only affect the displacement and water head of the rod end node, respectively. Therefore, it was considered that the displacement of the rod end node would not cause the PVD volume to change, and the change in the pore pressure of the node would also have no effect on the axial force of the PVD. By discretization of the continuity equation of the seepage of the PVD element, the combined matrix of mechanical stiffness and seepage for the PVD with a 2-node linear element can be obtained, as shown in Equation (4) [31]. Since the pore pressure at the node did not have a direction, the change caused by the direction of the seepage matrix did not need to be considered when the spatial transformation was performed. Therefore, Equation (4) can also be extended to the 3-dimensional matrix used for the 3-dimensional finite element simulation of the ground treatment with the PVD.

$$[\boldsymbol{K}] = \frac{A}{L}\begin{bmatrix} E & 0 & -E & 0 \\ 0 & -kt & 0 & kt \\ -E & 0 & E & 0 \\ 0 & kt & 0 & -kt \end{bmatrix} \tag{4}$$

where $[\boldsymbol{K}]$ is the combined stiffness matrix of the PVD; A is the cross-sectional area of the PVD; L is the length of the PVD; E is the modulus of elasticity of the PVD; k is the coefficient of permeability of the PVD; and t is the time.

4. Results and Discussion

4.1. Vertical Settlement Characteristics

The loading stages for various cross-sections were divided into four to eight levels to reliably consider the difference in the ground surface elevation and the soft soil settlement. For example, in section N5 + 850, the riprap loading process was divided into seven stages, as shown in Figure 6. The vertical settlements at the central axis of section N5 + 850 were obtained by CJP-3 and F-2 (Figure 4) monitoring data and plotted versus the results obtained numerically, as illustrated in Figure 6.

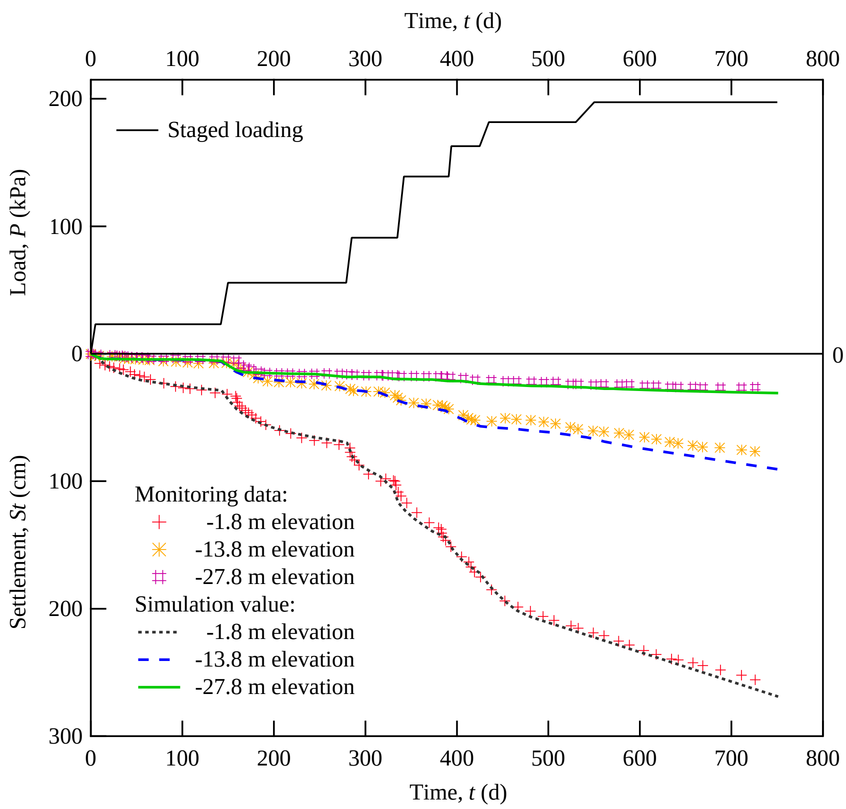

Figure 6. Monitoring and simulation curves of vertical settlements in section N5 + 850.

Figure 6 illustrates that the numerical simulation results agreed well with the monitoring data. Consequently, it can be concluded that the deployed model can accurately simulate the vertical settlement of soft soil ground treated by PVD-assisted staged riprap loading. The settlement of the surface and shallow soil layers had a similar stepped pattern following the applied staged loading. However, the gradual settlement pattern faded deeper in the soil profiles. Furthermore, according to the layered settlement monitoring data from three in situ observation sections, by accumulating the layered settlements in the PVD-treated zone (elevation from −1.8 m to −21.8 m) and the non-PVD zone (elevation from −21.8 m to −30.8 m), the vertical settlement in the PVD zone (S_{PVD}) and the non-PVD zone ($S_{non-PVD}$) were determined. It was found that S_{PVD} reached about 85% of the total settlement (S_{total}), while $S_{non-PVD}$ was limited to about 15% of S_{total}, as summarized in Table 5. The comparison suggested that the consolidation settlement occurred mainly in the PVD-treated zone.

Table 5. Statistics of layered settlements in the PVD-treated zone and the non-PVD zone.

Layered Settlement Monitoring Position	S_{PVD}/S_{total} (%)	$S_{non-PVD}/S_{total}$ (%)
F-1 in N3 + 850	84.4	15.6
F-2 in N3 + 850	87.4	12.6
F-3 in N3 + 850	85.6	14.4
F-1 in N5 + 850	80.4	19.6
F-2 in N5 + 850	85.9	14.1
F-3 in N5 + 850	86.6	13.4
F-1 in N11 + 050	83.2	16.8
F-2 in N11 + 050	86.1	13.9
F-3 in N11 + 050	82.7	17.3
Mean value	84.7	15.3

4.2. Horizontal Displacement Characteristics

The horizontal displacements at different elevations with time in CX-2 (Figure 4) of section N5 + 850, obtained from the monitoring data using an inclinometer and numerically, are plotted in Figure 7. It can be observed that the simulation results were in good agreement with the monitored data. Furthermore, the horizontal displacement mainly occurred in the PVD-treated zone, with a maximum displacement of 246 mm located at around −10 m elevation after 715 days of loading. This −10 m depth was equalt to about half of the used PVD length, while the horizontal displacement decreased sharply for the deeper soil layers and converged to zero at around −40 m elevation.

The filling height of the crest of the Lingni Seawall was higher than the berms, as shown in Figure 2. Before 130 d, the staged riprap loading was carried out simultaneously at the center and both sides (berms) of the embankment. When the berms reached the intended elevation, the riprap filling was stopped for the berms. After that, only the center part of the embankment continued to be riprap-loaded. Therefore, with the passage of construction time, the horizontal displacement curves in Figure 7 showed different variation trends due to different loading stages and time periods.

For −10 m (corresponding to the maximum displacement depth), the horizontal displacement increased with time and converged to a constant value after around 600 days. While for −26 m (representing the non-PVD zone), the horizontal displacement converged to a constant value only after 350 days, which mainly corresponded to the initial preloading stage, as shown in Figure 8.

4.3. Excess Pore Water Pressure Dissipation Regulations

The excess pore water pressure (Δu) at different elevations with time at K-2 of section N5 + 850, monitored using pore water pressure piezometers and obtained numerically, is plotted in Figure 9. It was found that the pore water pressure simulation results were consistent with the monitoring data. For the shallow soil ground in the PVD-treated zone, the pore water pressure increased quickly during the initial preloading stage and converged to zero once the loading became constant. Meanwhile, for the non-PVD zone, the excess pore water pressure increased slowly until reaching a constant value when the loading became constant for the deep soil layers and did not dissipate during the observation period. This phenomenon demonstrated the efficiency of utilizing PVDs to facilitate drainage for deep soft soils characterized by low permeability.

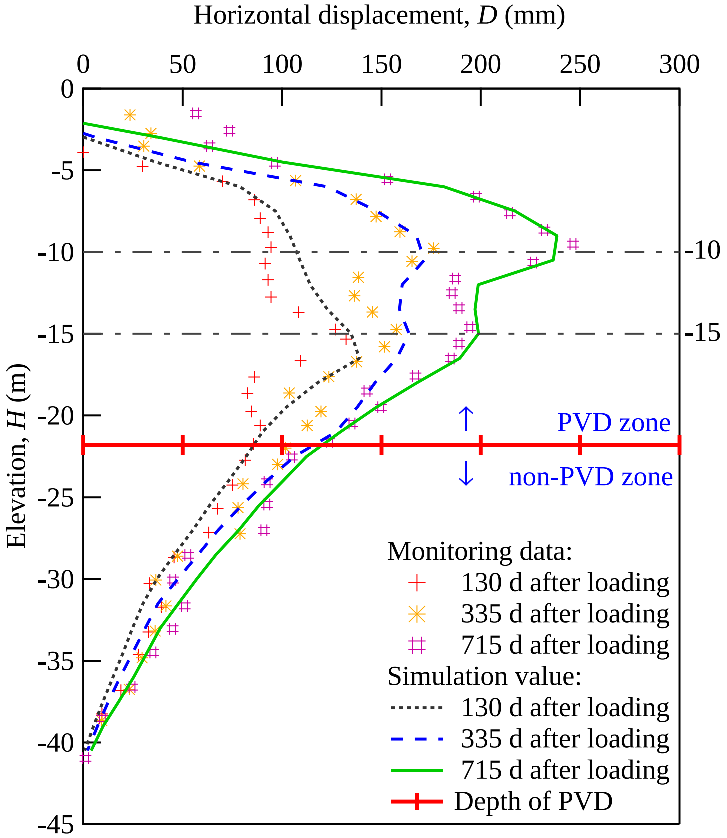

Figure 7. Monitoring and simulation curves of horizontal displacements in CX-2 of section N5 + 850.

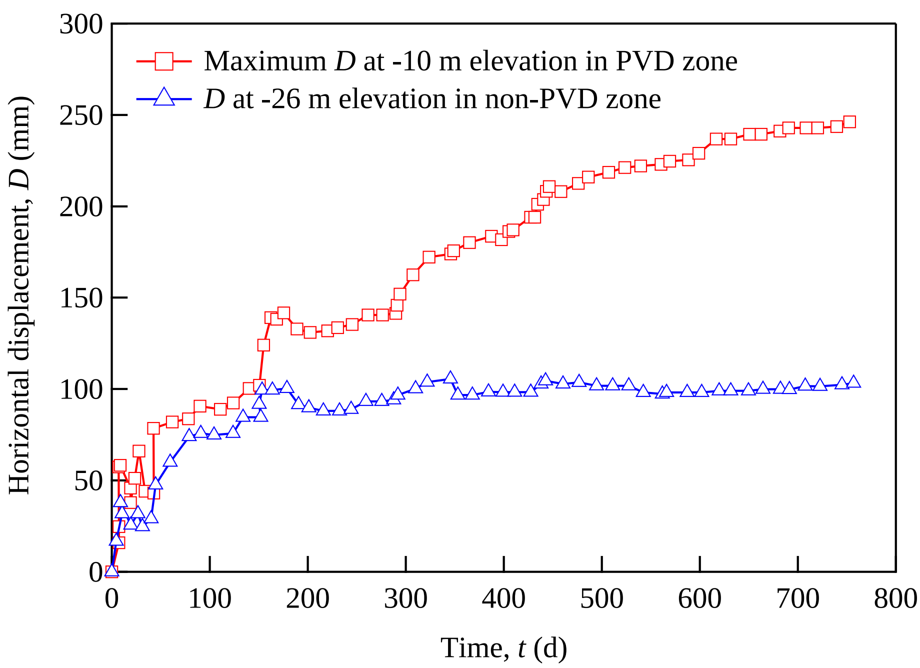

Figure 8. Horizontal displacements with time in CX-2 of section N5 + 850.

The deployed regulations of the excess pore water pressure dissipation utilizing the PVDs in the Lingni Seawall were investigated. Initially, the original consolidation state of the soft soil ground was analyzed under the hydrostatic water level and compared to the initial pore water pressure observations, as shown in Figure 10a. It can be observed that the initial pore water pressure almost coincided with the hydrostatic water pressure, which verified that the excess pore water pressure of the natural soil ground was almost zero. Then, by accumulating the increment in excess pore water pressure (Δu) at each staged loading (Δp), the relation curves between the cumulative excess pore water pressure ($\Sigma\Delta u$) and the load ($P = \Sigma\Delta p$) could be drawn, as shown in Figure 10b. It can be seen that $\Sigma\Delta u$ in the muck layer increased almost linearly with the load increase. The regulations for the excess pore water pressure dissipation induced by loading with PVD were analogous to previously reported field observations and model testing reports [33,34]. Further analysis showed a remarkable variation between the pore pressure coefficient ($\Delta u/\Delta p$) and the cumulative load ($\Sigma\Delta p$), as shown in Figure 10c.

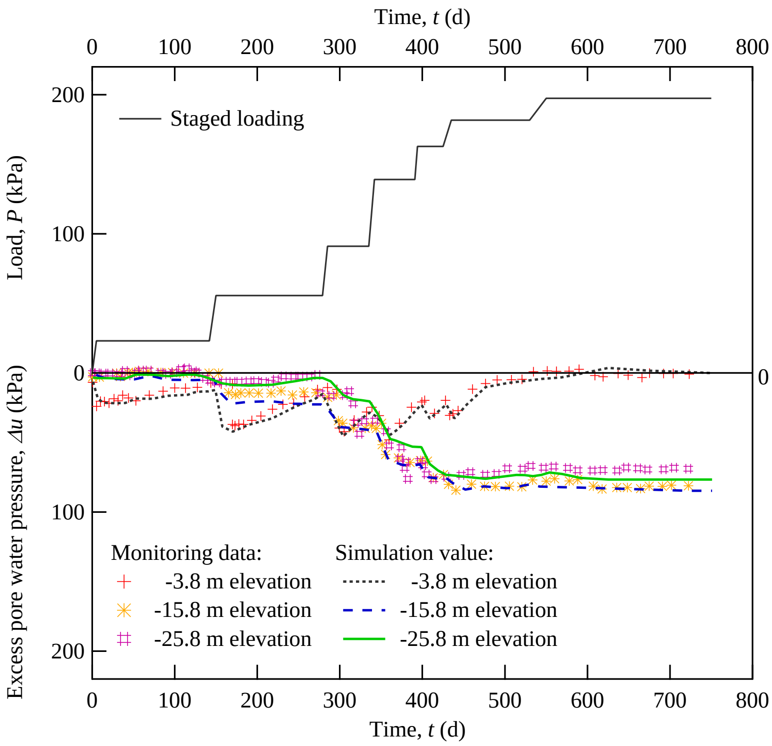

Figure 9. Monitoring and simulation curves of pore water pressure at K-2 of section N5 + 850.

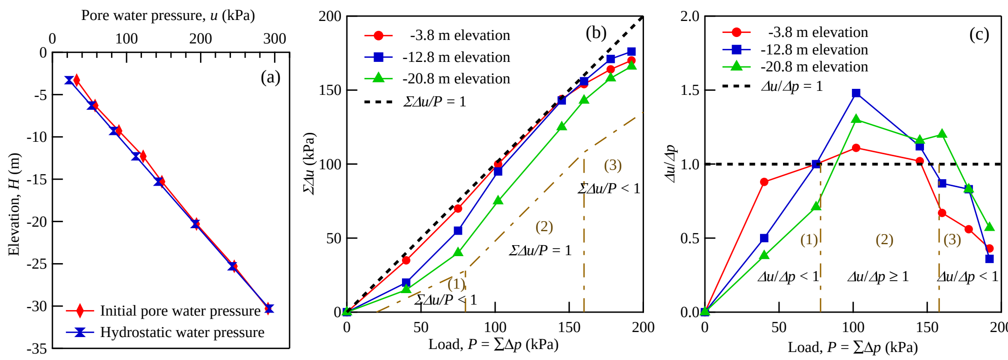

Figure 10. Excess pore water pressure dissipation regulations at K-2 of section N5 + 850: (**a**) Initial pore water pressure and hydrostatic water pressure; (**b**) Cumulative excess pore pressure with load; (**c**) Pore pressure coefficient with load.

In Figure 10b, $\Sigma\Delta u/P$ shows a three-period variation that was found to be similar to the $\Delta u/\Delta p$ variations illustrated in Figure 10c. In period 1 and period 3, the excess pore water pressure increment was less than the external load increment. During period 2, the excess pore water pressure increment was greater than or equal to the external load increment, as presented in Table 6. This was associated with the loading increment and rate during the staged loading. Among all the staged loadings, the fourth stage had the largest increment, resulting in a sharp increase in the excess pore water pressure within the muck layer, as demonstrated in Figure 9. Finally, it can be concluded that the staged loading rate and the riprap height can be controlled to ensure the safety and stability of the construction.

Table 6. The three-period variation in excess pore water pressure with load.

Variation Period	Loading Period	$\Sigma\Delta u/P$	$\Delta u/\Delta p$
Period 1	Initial loading period	<1	<1
Period 2	Mid-loading period	=1	≥1
period 3	End-loading period	<1	<1

4.4. Influence of the PVD on the Degree of Consolidation

In this study, the average radial degree of consolidation ($\overline{U}_r$) was calculated using the measured excess pore water pressure (u_{re}) [35]. However, u_{re} corresponds to a particular point and at a specific time (t) and might not represent the average excess pore water pressure ($\overline{u}_r$). Therefore, to calculate $\overline{U}_r$, the coefficient ζ was introduced for conversion, as shown in Equation (5) below:

$$\overline{U}_r = \frac{u_0 - \overline{u}_r}{u_0} = \frac{u_0 - \zeta \cdot u_{re}}{u_0} \tag{5}$$

where u_0 is the initiative excess pore water pressure; $\overline{u}_r$ is the average radial excess pore water pressure at time t; u_{re} is the measured excess pore water pressure at a particular point in time t; and $\zeta = \overline{u}_r/u_{re}$.

Then, coefficient ζ was obtained based on Barron's analytical solution (1948) [36] under a constant strain condition following Equations (6) and (7):

$$u_r = \frac{\overline{u}_r}{r_e^2 F_n}[r_e^2 ln(\frac{r}{r_w}) - \frac{r^2 - r_w^2}{2}] \tag{6}$$

$$F_n = \frac{n^2}{n^2 - 1} ln(n) - \frac{3n^2 - 1}{4n^2} \tag{7}$$

where u_r is the radial excess pore water pressure at time t at a radial distance r; t is the consolidation time; r is the radial distance from the central axis of the vertical drain well; r_e is the radius of the effective zone of drainage, as shown in Figure 2; r_w is the radius of the vertical drain well; and n is the drain spacing ratio, expressed as $n = r_e/r_w$.

Furthermore, by transforming Equation (6), we can obtain Equation (8). In the Lingni Seawall monitoring plan, the pore water pressure cells were embedded in the center of the effective zone of the PVDs; so, when $r = r_e$, $u_r = u_{re}$, coefficient ζ can be calculated using Equation (9) as follows:

$$\frac{\overline{u}_r}{u_r} = \frac{r_e^2 F_n}{r_e^2 ln(\frac{r}{r_w}) - \frac{r^2 - r_w^2}{2}} \tag{8}$$

$$\zeta = \frac{\overline{u}_r}{u_{re}} = \frac{r_e^2 F_n}{r_e^2 ln(\frac{r_e}{r_w}) - \frac{r_e^2 - r_w^2}{2}} \tag{9}$$

where the PVD equivalent radius r_w = 0.033 m adopted from Hansbo's solution (1979) [37]. For PVDs in a quincunx equilateral triangle pattern with interval spacing (l) of 1.5 m, the radius of the effective zone of the PVDs [38] r_e = 0.788 m; thus, n = 24. Finally, the coefficient ζ was found to equal 0.908.

Using Equation (5), $\overline{U}_r$ at the different elevation (H) was calculated for section N5 + 850 and is plotted in Figure 11. It can be observed that $\overline{U}_r$ obviously decreased with increase in the muck depth. The consolidation effect of the muck layer in the PVD zone was much better than that for the non-PVD zone. In particular, above −11.8 m elevation, corresponding to the half-length of the PVD, $\overline{U}_r$ reached up to 75–100%. The results showed that the PVD was efficient for accelerating the consolidation drainage for the soft soil layers; however, the effective depth of the PVD may be different due to the complexity of the prevailing engineering conditions and of the construction process. For example, in section N5 + 850, at the range extending from −11.8 m to −21.8 m elevation, $\overline{U}_r$ was limited to about 20–50%. However, in section N3 + 850 at −18 m elevation, $\overline{U}_r$ reached up to 80%. The result for the consolidation effectiveness agreed, in general, with the findings of previous research [39].

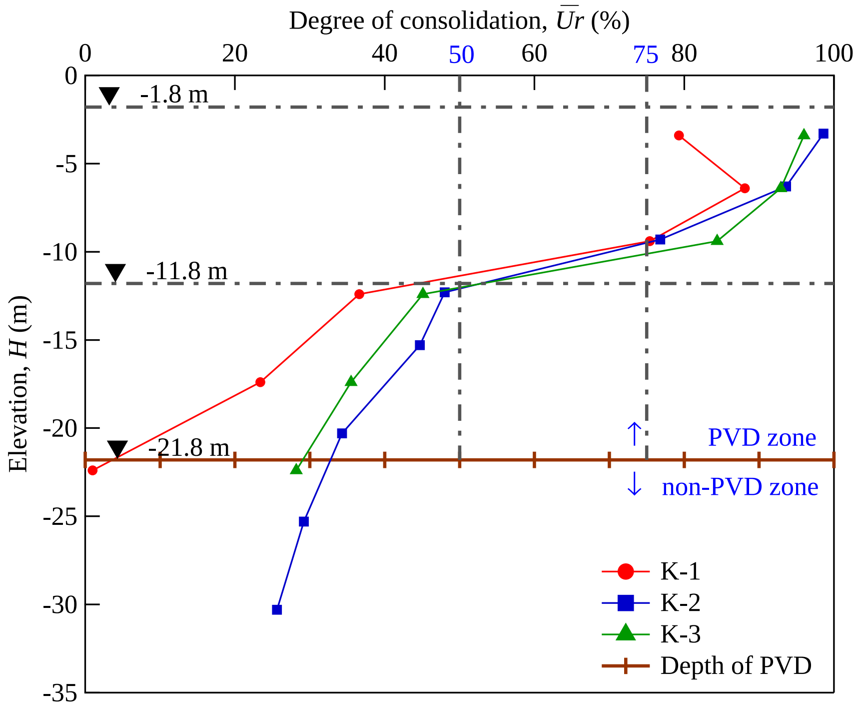

Figure 11. Degree of consolidation with elevation of section N5 + 850.

4.5. Consolidation Coefficient under PVD Performance

The PVD-assisted staged riprap preloading method involved draining the excess pore water from the surrounding soil layer during the consolidation associated with the hydraulic gradients induced by the embankment preloading. Thus, the water filling the pores flowed easily toward the PVD in the horizontal direction, and then travelled freely along the PVD vertically toward the permeable drainage layer on the ground surface. The consolidation coefficient of the soil layer will change during the loading and draining process, and the actual value of the consolidation coefficient will be different from that measured in the laboratory before construction. Therefore, back-analysis was used to optimize the design and the model parameters based on the monitoring data recorded during the embankment construction [40]. According to Carrillo's analytical solution (1942) [41] of the vertical drain model, the consolidation coefficient of the soil layers can be inversely calculated by the three-point method expressed in Equations (10) and (11) [42]. The three-point method is illustrated in Figure 12.

$$e^{\beta(t_2-t_1)} = \frac{S_2 - S_1}{S_3 - S_2} \tag{10}$$

$$\beta = \frac{1}{t_2 - t_1} \cdot ln(\frac{S_2 - S_1}{S_3 - S_2}) = \frac{2C_h}{F_n r_e^2} + \frac{\pi^2 C_v}{4{H_v}^2} \tag{11}$$

where β is the coefficient of the drain conditions; S_1, S_2 and S_3 are the settlements at time t_1, t_2 and t_3, respectively, and $t_2 - t_1 = t_3 - t_2$; F_n and r_e are annotated in Equations (6) and (7); C_v and C_h are the vertical and horizontal consolidation coefficients, respectively; and H_v is the vertical drain distance.

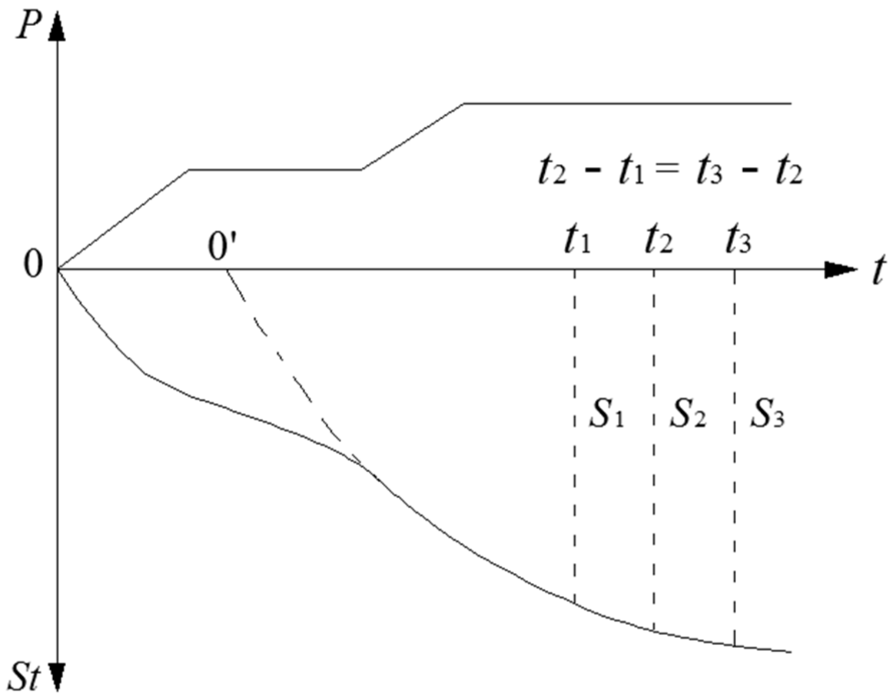

Figure 12. Three-point method for back-calculation of the consolidation coefficient.

Furthermore, by analyzing the experimental data from the oedometer tests using the square-root time method, the relationship between the vertical consolidation coefficient C_v and the horizontal consolidation coefficient C_h was determined with $C_h = 1.18C_v$ from our previous research [43]. Thus, the C_v and C_h values can be obtained using Equation (11) for each section, as summarized in Table 7. Comparing the back-calculation (bc) values of C_v (bc) and C_h (bc) to the values determined in the laboratory C_v (test) and C_h (test) [43], it was found that the inversely calculated value was larger than the test value. A good linear relationship was obtained by plotting the relation between the measured values versus the inversely calculated values, as shown in Figure 13.

Based on the relation illustrated in Figure 13, it was found that the drainage effect of the PVD and the riprap loading in the soft soil layers was accelerated, with the consolidation coefficient increasing by 1.4 times. The consolidation coefficient is a key parameter for consolidation calculation. It reflects the consolidation rate of soils. After PVD treatment, the consolidation rate of the soft soil ground was also obviously increased with increase in the consolidation coefficient in comparison to the non-PVD zone. Similar conclusions were also drawn in previous studies using back-analyses of the consolidation coefficient of PVD-improved soft clay from settlement data [44].

Table 7. Back-calculation of the consolidation coefficient.

Section	β (10^{-7} s^{-1})	C_v(bc) (10^{-4} cm^2/s)	C_h(bc) (10^{-4} cm^2/s)
N3 + 850	1.768	10.86	12.82
N5 + 850	1.491	9.17	10.82
N11 + 050	1.556	9.56	11.28

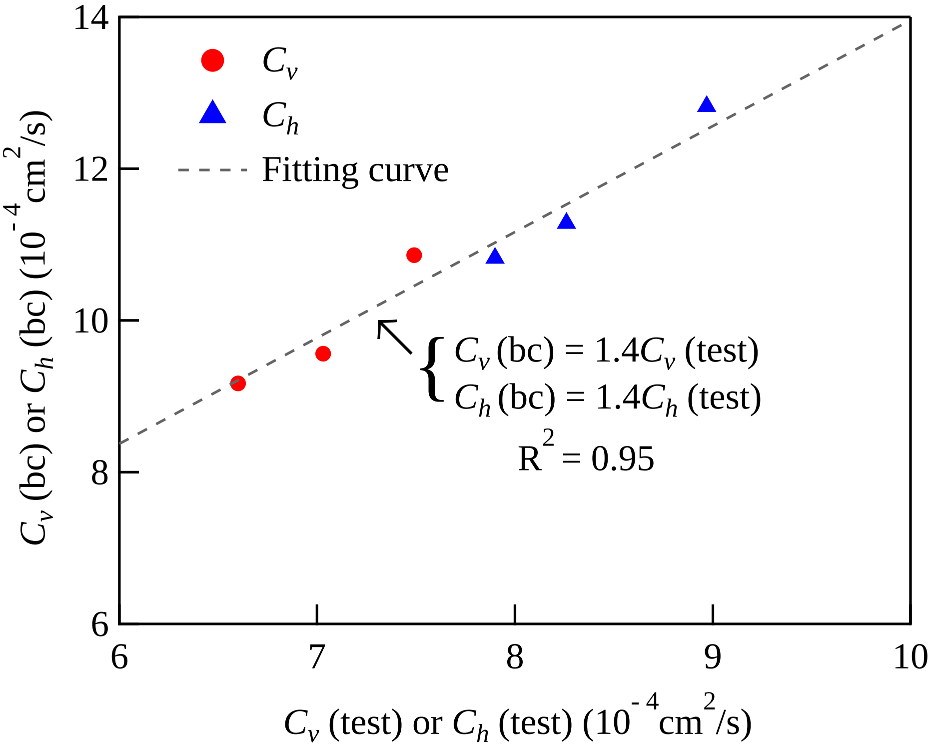

Figure 13. Relationship between back-calculation values and test values of the consolidation coefficient.

4.6. Strength Improvement under PVD Performance

A series of in situ vane shear tests were conducted on the natural muck soil before loading and at six different holes after staged loading to investigate the strength development of the reinforced ground. Holes VST-1, VST-2, and VST-3 correspond to after the berm loading stage, while holes VST-4, VST-5, and VST-6 (Figure 4) correspond to the full riprap loading conditions. The in situ vane shear strength results from section N5 + 850 are depicted in Figure 14. The strength development in the PVD zone was found to be greater than that in the non-PVD zone. Moreover, the strength improvement at the central axis was greater than that at the berms. Especially, at shallower than −11.8 m elevations, corresponding to the half-length of the PVD, the soil strength increased significantly up to 200–700%. The strength increased by 60–150% in the range of −11.8 m to −21.8 m elevation in the PVD zone. This pattern was analogous to the verified consolidation and settlement results, reflecting the strength improvement and ground stability. It must be noted that similar strength variation trends in vertical drain-improved clay deposits subjected to vacuum or surcharge loading have been reported in the literature [45,46].

4.7. Error and Evaluation Metrics Analysis of Numerical Simulation

To further evaluate the accuracy of the numerical simulation model, the mean absolute error (MAE) and the coefficient of determination or R-squared (R^2) were calculated, as presented in Table 8. All the simulation data had smaller MAE (1.870–7.461) and higher R^2 (0.962–0.998), which indicated that the model used and the assigned boundaries accurately estimated the vertical settlement, horizontal displacement, and excess pore water pressure. Compared with the totally solid element model, with the R^2 from 0.914 to 0.977 [30], the model accuracy and calculating efficiency were increased, and the numbers of elements and nodes were reduced by using the PVD linear element.

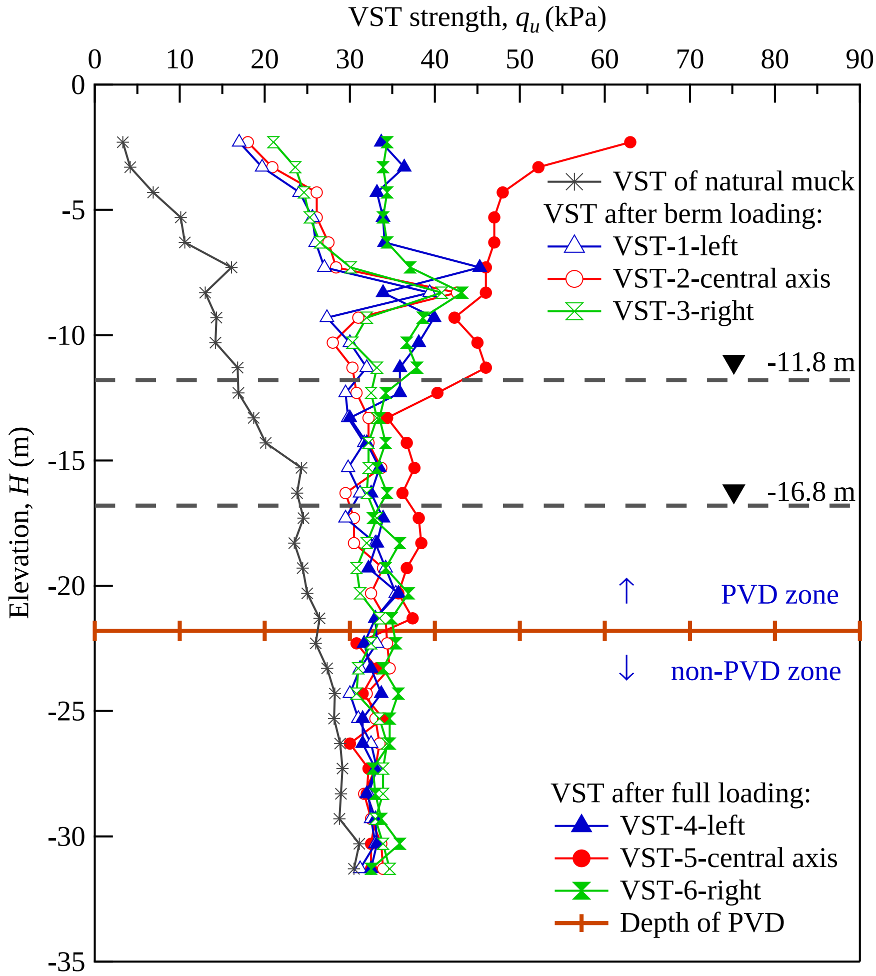

Figure 14. In situ vane shear strength in section N5 + 850.

Table 8. Error and evaluation metrics analysis of numerical simulation model.

Parameter	Elevation or Time	MAE	R^2
Vertical settlement	−1.8 m	2.850	0.998
	−13.8 m	2.690	0.994
	−27.8 m	2.153	0.962
Horizontal displacement	130 d	7.461	0.979
	335 d	6.456	0.990
	715 d	5.802	0.991
Excess pore water pressure	−3.8 m	1.870	0.977
	−15.8 m	3.491	0.983
	−25.8 m	3.016	0.980

5. Conclusions

In situ monitoring and measurement, numerical simulation, analytical calculation and back-calculation, and theoretical analysis were conducted to assess the consolidation, settlement, deformation and strength characteristics of marine soft soil ground treated by staged riprap combined with PVD. The conclusions drawn are as follows:

(1) The PVD-assisted riprap showed a good improvement effect for deep marine soft soil ground. In particular, in the PVD-treated zone within 10 m in depth, corresponding

to the half-length of the PVD, the average radial degree of consolidation reached up to 75–100%, and the soil strength increased significantly by 200–700%.

(2) $\Sigma\Delta u/P$ showed a three-period variation that was found to be similar to the $\Delta u/\Delta p$ variations. Thus, the staged loading rate and the riprap height can be controlled to ensure the safety and stability of the seawall construction.

(3) The numerical simulation data were closely aligned with the engineering accuracy requirements and showed a high level of consistency with the monitored data. Compared with the totally solid element model, a self-defined PVD linear 1-dimensional drain element reduced the numbers of elements and nodes, and increased the calculating efficiency and model accuracy.

(4) However, since this study focused on a 2-dimensional embankment numerical simulation with a 1-dimensional drain element of PVD, the accuracy and applicability of 3-dimensional modeling of embankments with a linear element of PVD remains to be investigated and verified through more engineering case studies.

Author Contributions: Conceptualization, X.-T.W.; methodology, X.-T.W. and Z.-M.X.; software, J.-N.L. and Z.-M.X.; validation, J.-N.L.; formal analysis, X.-T.W.; investigation, X.-T.W. and J.-N.L.; data curation, X.-T.W., J.-N.L. and Z.-M.X.; writing—original draft preparation, X.-T.W.; writing—review and editing, X.-T.W. and J.-N.L.; visualization, J.-N.L. and Z.-M.X. All authors have read and agreed to the published version of the manuscript.

Funding: This research was funded by the National Natural Science Foundation of China (Grant Number 52178370 and 41602319), and the China Scholarship Council (Grant Number 202006415016).

Data Availability Statement: The data presented in this study are available on request from the corresponding author. The data are not publicly available due to ongoing research.

Acknowledgments: The authors are indebted to the First Highway Consultants Company Limited of the China Communications Construction Company and the Wenzhou Traffic and Transportation Bureau for their assistance in the field investigations of this project.

Conflicts of Interest: The authors declare no conflicts of interest. The funders had no role in the design of the study; in the collection, analyses, or interpretation of data; in the writing of the manuscript, or in the decision to publish the results.

References

1. Nazir, R.; Moayedi, H.; Subramaniam, P.; Ghareh, S. Ground improvement using SPVD and RPE. *Arab. J. Geosci.* **2017**, *10*, 1–21. [CrossRef]
2. Xia, C.Q.; Deng, Y.B.; Zhu, M.; Niu, J.J.; Zheng, L.K.; Chen, X.S. One-dimensional solar energy thermal consolidation model testing and analytical calculation for marine soft clays. *J. Mar. Sci. Eng.* **2022**, *10*, 1634. [CrossRef]
3. Tang, J.F.; Xu, J.K.; Zhou, D.Z.; Huang, D.; Zeng, K.; Li, Y.H.; Chen, Z. Ground surface deformation caused by pipe jacking construction in a soft soil area: An experiment-based study. *Buildings* **2023**, *13*, 1628. [CrossRef]
4. Terzaghi, K. *Erdbaumechanik auf Bodenphysikalischer Grundlage*; Franz Deuticke: Leipzig, Germany; Wien, Austria, 1925.
5. Hore, R.; Chakraborty, S.; Ansary, M.A. A field investigation to improve soft soils using prefabricated vertical drain. *Transp. Infrastruct. Geotechnol.* **2020**, *7*, 127–155. [CrossRef]
6. Cascone, E.; Biondi, G. A case study on soil settlements induced by preloading and vertical drains. *Geotext. Geomembr.* **2013**, *38*, 51–67. [CrossRef]
7. Prabavathy, S.; Rajagopal, K.; Pitchumani, N. Investigation of smear zone around PVD mandrel using image-based analysis. *Int. J. Geosynth. Ground Eng.* **2021**, *7*, 1–16. [CrossRef]
8. Deng, Y.B.; Liu, G.B.; Lu, M.M.; Xie, K.H. Consolidation behavior of soft deposits considering the variation of prefabricated vertical drain discharge capacity. *Comput. Geotech.* **2014**, *62*, 310–316. [CrossRef]
9. Al-Homoud, A.S.; Tanash, N. Monitoring and analysis of settlement and stability of an embankment dam constructed in stages on soft ground. *Bull. Eng. Geol. Environ.* **2001**, *59*, 259–284. [CrossRef]
10. Bo, M.W.; Arulrajah, A.; Horpibulsuk, S.; Chinkulkijniwat, A.; Leong, M. Laboratory measurements of factors affecting discharge capacity of prefabricated vertical drain materials. *Soils Found.* **2016**, *56*, 129–137. [CrossRef]
11. Skempton, A.W.; Peck, R.B.; MacDonald, D.H. Settlement analyses of six structures in Chicago and London. *Proc. Inst. Civ. Eng.* **1955**, *4*, 525–542. [CrossRef]

12. Liu, S.Y.; Cai, G.J.; Puppala, A.J.; Tu, Q.Z. Prediction of embankment settlements over marine clay using piezocone penetration tests. *Bull. Eng. Geol. Environ.* **2011**, *70*, 401–409. [CrossRef]
13. Cheng, Y.; Cai, X.C.; Mo, H.Z.; Gu, M.X. Numerical analysis on the behavior of floating geogrid-encased stone column improved foundation. *Buildings* **2023**, *13*, 1609. [CrossRef]
14. Arulrajah, A.; Bo, M.; Leong, M.; Disfani, M. Piezometer measurements of prefabricated vertical drain improvement of soft soils under land reclamation fill. *Eng. Geol.* **2013**, *162*, 33–42. [CrossRef]
15. Park, H.I.; Kim, K.S.; Kim, H.Y. Field performance of a genetic algorithm in the settlement prediction of a thick soft clay deposit in the southern part of the Korean peninsula. *Eng. Geol.* **2015**, *196*, 150–157. [CrossRef]
16. Namazi, E.; Mohamad, H.; Jorat, M.E.; Hajihassani, M. Investigation on the effects of twin tunnel excavations beneath a road underpass. *Electron. J. Geotech. Eng.* **2011**, *16*, 1–8.
17. Han, K.H.; Wang, L.; Su, D.; Hong, C.Y.; Chen, X.S.; Lin, X.T. An analytical model for face stability of tunnels traversing the fault fracture zone with high hydraulic pressure. *Comput. Geotech.* **2021**, *140*, 104467. [CrossRef]
18. Li, A.L.; Rowe, R.K. Combined effects of reinforcement and prefabricated vertical drains on embankment performance. *Can. Geotech. J.* **2001**, *38*, 1266–1282. [CrossRef]
19. Parsa-Pajouh, A.; Fatahi, B.; Vincent, P.; Khabbaz, H. Trial embankment analysis to predict smear zone characteristics induced by prefabricated vertical drain installation. *Geotech. Geol. Eng.* **2014**, *32*, 1187–1210. [CrossRef]
20. Chai, J.C.; Miura, N. Investigation of factors affecting vertical drain behavior. *J. Geotech. Geoenviron. Eng.* **1999**, *125*, 216–226. [CrossRef]
21. Lu, M.M.; Sun, J.X. Analytical model for consolidation of soft ground improved by PVDs with air-boosted system. *Comput. Geotech.* **2022**, *151*, 104968. [CrossRef]
22. Maleki, M.; Alielahi, H.; Rahmani, I. Effect of smear zone characteristics on PVD-improved soft soils using field data and numerical simulations. *Indian Geotech. J.* **2022**, *52*, 1391–1409. [CrossRef]
23. Lin, S.; Fu, D.F.; Zhou, Z.F.; Yan, Y.; Yan, S.W. Numerical investigation to the effect of suction-induced seepage on the settlement in the underwater vacuum preloading with prefabricated vertical drains. *J. Mar. Sci. Eng.* **2021**, *9*, 797. [CrossRef]
24. Kan, M.E.; Indraratna, B.; Rujikiatkamjorn, C. On numerical simulation of vertical drains using linear 1-dimensional drain elements. *Comput. Geotech.* **2021**, *132*, 103960. [CrossRef]
25. *GB 50021-2001*; Code for Investigation of Geotechnical Engineering. China Architecture & Building Press: Beijing, China, 2009.
26. Wu, X.T. Study on Engineering Properties and Consolidation Settlement Regularity of Soft-Soil in Wenzhou Shoal. Ph.D. Thesis, China University of Geosciences, Wuhan, China, 2010.
27. *SL 551-2012*; Technical Specification for Earth-Rockfill Dam Safety Monitoring. China Water & Power Press: Beijing, China, 2012.
28. Ye, G.B.; Xu, Y.; Zhang, Z. Performance evaluation of PVD-reinforced soft soil with surcharge and vacuum preloading. *Int. J. Civ. Eng.* **2018**, *16*, 421–433. [CrossRef]
29. Jiang, M.; Bian, X.C.; Wu, J.G.; Jian-Wu, H.; Chen, Y.M.; Chen, R.P. Field measurement and numerical simulation of estuarine deposit settlements under embankment loads. *Chin. J. Rock Mech. Eng.* **2010**, *29*, 1060–1067.
30. Zhan, X.J.; Gao, C.S.; Zhu, Q.F.; Yang, S.H.; Pang, B. Numerical analysis of breakwater construction on soft clay in harbor area of Lianyungang Port. *Chin. J. Geotech. Eng.* **2017**, *39*, 2109–2115.
31. Fei, K.; Zhang, W.J. *ABAQUS Application in Geotechnical Engineering*; China Water & Power Press: Beijing, China, 2010.
32. Wood, D.M. *Soil Behaviour and Critical State Soil Mechanics*; Cambridge University Press: Cambridge, UK, 1990.
33. Lorenzo, G.; Bergado, D.; Bunthai, W.; Hormdee, D.; Phothiraksanon, P. Innovations and performances of PVD and dual function geosynthetic applications. *Geotext. Geomembr.* **2004**, *22*, 75–99. [CrossRef]
34. Chen, H.; Chu, J.; Guo, W.; Wu, S.F. Land reclamation using the horizontal drainage enhanced geotextile sheet method. *Geotext. Geomembr.* **2023**, *51*, 131–150. [CrossRef]
35. Hou, J.F. *Calculation of Consolidation Degree of Soil Mass with Pore Water Pressure Measured in Vacuum Preloading Works*; China Harbour Engineering: Hong Kong, China, 2005; pp. 13–15.
36. Barron, R.A. Consolidation of fine-grained soils by drain wells by drain wells. *Trans. Am. Soc. Civ. Eng.* **1948**, *113*, 718–742. [CrossRef]
37. Hansbo, S. Consolidation of clay by bandshaped prefabricated drains. *Ground Eng.* **1979**, *12*, 16–27.
38. Liu, Z.; Gao, Y.; Liao, J.; Zhou, C.Y. Stochastic medium model for the settlement calculation of prefabricated vertical drains of soft soil foundations in the coastal area of south China. *J. Mar. Sci. Eng.* **2022**, *10*, 867. [CrossRef]
39. Ong, C.Y.; Chai, J.C.; Hino, T. Degree of consolidation of clayey deposit with partially penetrating vertical drains. *Geotext. Geomembr.* **2012**, *34*, 19–27. [CrossRef]
40. Huang, S.; Huang, J.S.; Kelly, R.; Jones, M.; Kamruzzaman, A. Predicting settlement of embankments built on PVD-improved soil using Bayesian back analysis and elasto-viscoplastic modelling. *Comput. Geotech.* **2023**, *157*, 105323. [CrossRef]
41. Carrillo, N. Simple two and three dimensional case in the theory of consolidation of soils. *J. Math. Phys.* **1942**, *21*, 1–5. [CrossRef]
42. Zeng, G.X.; Yang, X.L. Settlement analysis of sand-drained ground. *J. Zhejiang Univ.* **1959**, *3*, 34–72.
43. Wu, X.T. Research on relation between consolidation coefficient and consolidation stress of silt in Wenzhou shoal. *Rock Soil Mech.* **2013**, *34*, 1675–1680.
44. Voottipruex, P.; Bergado, D.; Lam, L.; Hino, T. Back-analyses of flow parameters of PVD improved soft Bangkok clay with and without vacuum preloading from settlement data and numerical simulations. *Geotext. Geomembr.* **2014**, *42*, 457–467. [CrossRef]

45. Chai, J.C.; Shen, J.S.L.; Liu, M.D.; Yuan, D.J. Predicting the performance of embankments on PVD-improved subsoils. *Comput. Geotech.* **2018**, *93*, 222–231. [CrossRef]
46. Zhang, Z.; Ye, G.B.; Xu, Y. Comparative analysis on performance of vertical drain improved clay deposit under vacuum or surcharge loading. *Geotext. Geomembr.* **2018**, *46*, 146–154. [CrossRef]

Disclaimer/Publisher's Note: The statements, opinions and data contained in all publications are solely those of the individual author(s) and contributor(s) and not of MDPI and/or the editor(s). MDPI and/or the editor(s) disclaim responsibility for any injury to people or property resulting from any ideas, methods, instructions or products referred to in the content.